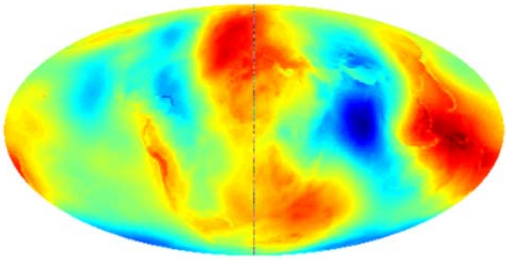

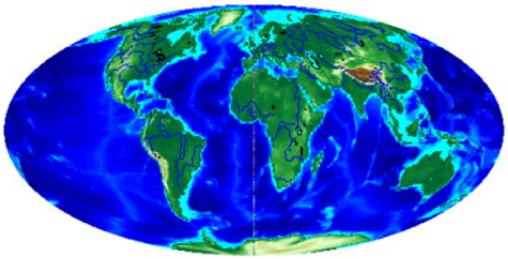

Siegen Preprints on Geomathematics

Inverting GRACE Gravity Data for Local Climate Effects

D. Fischer and V. Michel

Geomathematics Group
Department of Mathematics
University of Siegen
Germany

www.geomathematics-siegen.de

9

Inverting GRACE gravity data for local climate effects

D. Fischer and V. Michel
Geomathematics Group, University of Siegen, Germany
www.geomathematics-siegen.de
Email: michel@mathematik.uni-siegen.de

June 19, 2012

Abstract

The Amazon area is the largest water shed on Earth. Thus, it is of great importance to observe the water levels regularly. The satellite mission Gravity Recovery and Climate Experiment (GRACE) allows, since its launch in 2002, a monthly global overview of the water distribution on Earth, in particular floods and droughts. In recent years, the Amazon area has experienced a number of extreme weather situations in late summer (July through October), explicitly a drought in 2005 and one in 2010. Furthermore, one can identify the remains of a flood in spring 2009 in the summer season of 2009 as well. Here we present corresponding results with respect to a new localized method called the RFMP that can be applied to ill-posed inverse problems. In comparison to the usual processing of GRACE data as well as other data types (i.e. the volumetric soil moisture content given by the NOAA-CIRES Twentieth Century Global Reanalysis Version II and the average layer 1 soil moisture given by the GLDAS Noah Land Surface Model L4), we gain an improved spatial resolution with the novel method.

1 Introduction

The GRACE gravity mission (Gravity Recovery and Climate Experiment, see [17]), which was launched in 2002, has allowed the recovery and exploration of estimates of regional and temporal variations of water masses in the form of ground water, soil water, surface water, and snow pack for the first time. Moreover, the data is given as monthly potentials of the whole surface of the Earth. Thus, we may use time-scales from one month to several years. Currently, there are 9 years of useful and comparable data to analyze interannual (e.g. seasonal) and long-term (e.g. the mass loss in Greenland over the last six years) changes in our climate system that allow for a better understanding of the global water cycle, and especially of droughts and floods. However, for direct data on a

supraregional or global scale we still rely on simulations from hydrology models which are only given in a poor resolution.
The combination of these hydrology models with constraints from the GRACE gravity mission results in a better resolution (see [25, 28, 29]). Furthermore, the monthly gravity maps of GRACE were improved by using more sophisticated background geophysical models and data processing techniques, which leads to a resolution better than 300 km in the reprocessed GRACE release 4 used in this work (see [5, 7]). Because of these improvements of the resolution it was possible to resolve, e.g., the Amazon watershed from smaller systems in the north when researching seasonal mass changes in South America (see, e.g., [14, 28]).
While other major river systems have been analyzed as well including the Congo basin [9], the Mississippi river basin [26], the Yangtze river basin [18], and the Zambezi river basin [30], we can record a concentration on the Amazon river (see, e.g., [4, 7, 8, 10, 27, 28]), which was observed for different periods of time with different techniques. The Amazon area is the largest water shed on Earth and, thus, has a major influence on the global climate, sea levels, and temperatures. Extreme weather events like floods and droughts do not only have an enormous impact on the population in the Amazon area but on the whole water cycle. For this reason, a detailed and consecutive investigation of such phenomena is of great importance. We use here a novel technique called the RFMP to locate and analyze extreme weather events of the late summer months of six successive years starting with 2005 in the Amazon area, where the novel method allows for a much better localization and resolution of these effects than the usual methods or hydrological data.
After a short introduction of the used data set and the RFMP, we concentrate on localizing extreme weather conditions in inverted GRACE potentials. Here, we invert for the density distribution, since it represents large-scale floods and droughts very clearly. A comparison with other methods and other data sets shows the superiority of the novel method in combination with satellite gravity data with respect to the resolution and location of such extreme weather events.

2 Preliminaries

The Euclidean space $\mathbb{R}^l$ is equipped with the usual dot product

$$\langle x, y\rangle_{\mathbb{R}^l} := \sum_{j=1}^{l} x_j y_j, \quad x, y \in \mathbb{R}^l,$$

and its induced norm

$$||x||_{\mathbb{R}^l} := \sqrt{\langle x, x\rangle_{\mathbb{R}^l}}.$$

Furthermore, the closed ball with radius $a > 0$ is denoted by $\mathcal{B} := \{x \in \mathbb{R}^3 | \, |x| \leq a\}$. Moreover, $\mathrm{L}^2(\mathcal{B})$ denotes the space of all square-integrable scalar functions on $\mathcal{B}$, i.e. all $F : \mathcal{B} \to \mathbb{R}$ with

$$||F||_{\mathrm{L}^2(\mathcal{B})} := \left(\int_{\mathcal{B}} [F(x)]^2 \mathrm{d}x \right)^{1/2} < \infty.$$

The inner product for $\mathrm{L}^2(\mathcal{B})$ is defined by

$$\langle F, G\rangle_{\mathrm{L}^2(\mathcal{B})} := \int_{\mathcal{B}} F(x)G(x)\mathrm{d}x, \quad F, G \in \mathrm{L}^2(\mathcal{B}).$$

2.1 The Problem: Inverse Gravimetry

Gaining information about the distribution of, e.g., water masses in the upper layer of the Earth out of satellite data involves solving Newton's law of gravitation

$$V(x) = \gamma \int_{\mathcal{B}} \frac{\rho(y)}{|x-y|}\ \mathrm{d}y,\ x \in \mathbb{R}^3 \setminus \mathcal{B},$$

for the density distribution ρ, where γ is the gravitational constant and V is the gravitational potential. This problem is ill-posed for several reasons: The solution is not unique. One possible model assumption for a unique solution is a harmonicity constraint on ρ. This a-priori condition (as all other known possibilities) lacks a physical interpretation but has a mathematical justification (see the survey article [24] for further details). Moreover, the (harmonic) solution ρ discontinuously depends on V, i.e. it is unstable. Thus, we need to use a regularization method to get a stable approximation for ρ.
In the following, we represent the relation between the density and the gravitational potential by functionals $\mathcal{F}^k$, i.e.

$$\mathcal{F}^k\ \rho := \int_{\mathcal{B}} \frac{\rho(y)}{|x_k-y|}\ \mathrm{d}y \in \mathbb{R}$$

where $\rho \in \mathrm{L}^2(\mathcal{B})$ and $x_k \in \mathbb{R}^3 \setminus \mathcal{B}$ (see [22] for a series representation).

2.2 The Data: GRACE Release 4

GRACE data has been provided by different research groups. In this work, we will use the monthly data provided by the Jet Propulsion Laboratory (JPL, see [19], Release 04), which is given in spherical harmonics coefficients up to degree and order 60. To analyze the temporal variations, we observe the mean potentials V_a of the late summer months (July to October) for each of the years $a = 2005, \ldots, 2010$, where we denoise the potentials with Freeden wavelets of the cp type (see below). Since we want to reconstruct the mass variations directly, we subtract the mean potential V_{mean} (the mean value of all V_a) from each potential V_a and use this difference as an input to our novel algorithm to detect local changes in the masses on Earth.
However, it is well-known that the higher degrees and orders of the GRACE potentials contain noise that needs to be removed by some kind of smoothing. Note that smoothing also attenuates the real signal such that we have to expect a change in magnitudes. In [28], a smoothing function with an effective Gaussian radius was suggested. Furthermore, in [20, 21] a probabilistic decorrelation

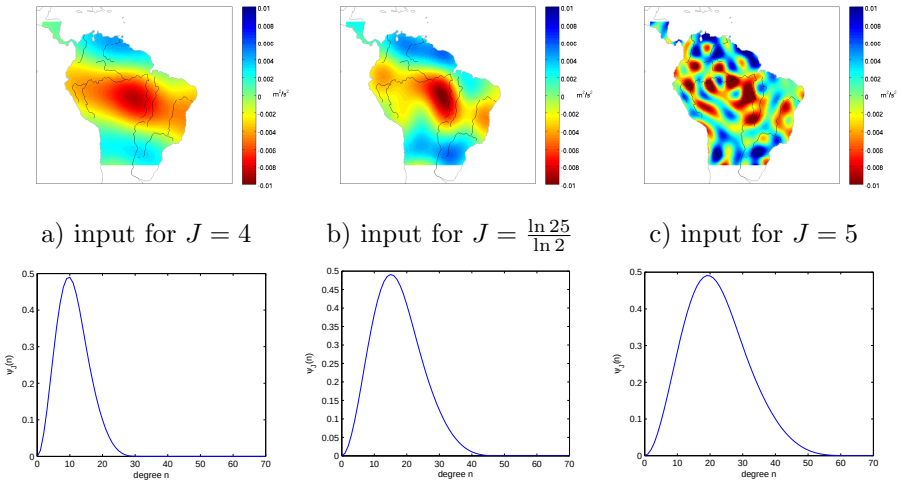

a) input for $J = 4$ b) input for $J = \frac{\ln 25}{\ln 2}$ c) input for $J = 5$

d) $\psi_J(n)$ for $J = 4$ e) $\psi_J(n)$ for $J = \frac{\ln 25}{\ln 2}$ f) $\psi_J(n)$ for $J = 5$

Figure 1: Input $V_{2010} - V_{\text{mean}}$ (top row) at scales $J = 4$, $J = \frac{\ln 25}{\ln 2}$, and $J = 5$ as well as the cubic polynomial filter functions $\psi_J(n)$ for $J = 4$, $J = \frac{\ln 25}{\ln 2}$, and $J = 5$ in the bottom row

method is developed to remove correlated and resolution dependent noise in the data coefficients (i.e. GRACE striping). Such filter coefficients are given for three different degrees of smoothing.
For our investigations, we prefer spherical wavelets (see [15, 16]) to analyze variations in the gravitational potential of the Earth. For this particular application, this can easily be implemented by calculating the filtered expansion

$$\sqrt{4\pi}\,\frac{\gamma M}{a}\sum_{n=3}^{E_n}\sum_{j=-n}^{n}\psi_J(n)\tilde{V}_{n,j}Y_{n,j}\left(\frac{x}{|x|}\right)$$

to reconstruct the data from the given spherical harmonics coefficients $\tilde{V}_{n,j}$, where M is the Earth's mass and E_n is the maximal degree of the coefficients. Here, $Y_{n,j}$ represents the (fully normalized) real spherical harmonics.
As suggested in [10], we use the P-wavelet

$$\psi_J(n) = \sqrt{(\varphi_{J+1}(n)^2) - (\varphi_J(n))^2}$$

corresponding to the cubic polynomial scaling function $\varphi_J(n)$ defined as

$$\varphi_J(n) = \begin{cases} (1-2^{-J}n)^2(1+2^{-J+1}n) & ,0 \le n < 2^J \\ 0 & ,n \ge 2^J \end{cases}$$

as a filter (see also [15]). It controls up to which degree and to what extent the coefficients of the spherical harmonics are considered (see the bottom row of

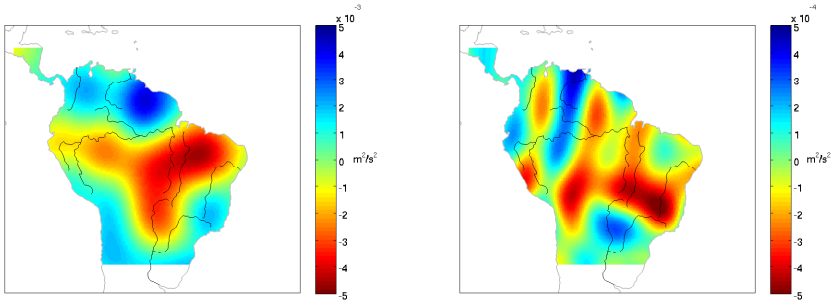

a) input for $J = \frac{\ln 23}{\ln 2}$

b) difference of a) to the input for $J = \frac{\ln 25}{\ln 2}$

Figure 2: Input $V_{2007} - V_{\text{mean}}$ at scale $J = \frac{\ln 23}{\ln 2}$ and difference to the input $V_{2007} - V_{\text{mean}}$ at scale $J = \frac{\ln 25}{\ln 2}$

figure 1). Both low and high coefficients are weighted less than the coefficients in between. Nonetheless, an increasing scale J admits more detail information. However, it bears the risk to include errors or artefacts like satellite tracks as well. Thus, it has to be investigated carefully which filter yields a realistic and useful viable input. In [10], scale $J = 4$ (no coefficients above degree 31 are considered) was suggested, since $J = 5$ (no coefficients above degree 63 are considered) is already contaminated with noise (see a) and c) in figure 1). We believe that a good compromise can be achieved by choosing the scale $J = \frac{\ln 25}{\ln 2}$ (see figure 1 b) and e)), where the coefficients up to degree 49 are taken into account. Now we expect that there are enough details included to recover the desired effects where the contained noise is still suppressed sufficiently.
However, this choice is only applicable if we invert a potential with a large signal to noise ratio. In the years 2006 to 2008 there are no extreme weather situations to be recovered. Thus, the signal to noise ratio decreases and we recover the infamous stripes of GRACE data (confer figure 6). As a consequence, we filter the data more strongly by using the cubic polynomial wavelet filter with parameter $J = \frac{\ln 23}{\ln 2}$ which corresponds to a weighted use of all coefficients up to degree 45. In figure 2, we display the used potential for $J = \frac{\ln 23}{\ln 2}$ (see figure 2 a)) as well as the difference to the potential filtered with a wavelet filter with $J = \frac{\ln 25}{\ln 2}$ (see figure 2 b)) in the case of summer 2007. Clearly, we lose some of the stripes in the potential and gain a signal with a better signal to noise ratio as an input to our inversion.
Subsequently, we use scale $J = \frac{\ln 25}{\ln 2}$ to filter the input of the years 2005, 2009, and 2010, which are the years with large signals in the GRACE potential that dominate the noise. The years 2006 to 2008 are filtered with scale $J = \frac{\ln 23}{\ln 2}$ to gain an input, where the signal is not disturbed by stripes.

2.3 The Method: Regularized Functional Matching Pursuit (RFMP)

Since we want to recover the mass density distribution ρ out of the gravitational potential given by GRACE data (which corresponds to ρ and is measured at a particular point x_i outside the Earth), we have to solve an inverse problem, where the data is given in terms of a (linear) functional $\mathcal{F}^i$ applied to the target function ρ, i.e. the data are $y_i = \mathcal{F}^i\rho$, $i = 1, \dots, l$, where ρ is unknown.
The main idea is to find a representation for ρ in terms of all kinds of different trial functions to best match the signal $\mathcal{F}\rho$, where we collect all functionals in the operator $\mathcal{F}\rho := (\mathcal{F}^1\rho, \dots, \mathcal{F}^l\rho)$. All the available trial functions are collected in a set called the dictionary $\mathcal{D}$. Now in every step, the iterative method chooses that trial function d out of $\mathcal{D}$ and the corresponding coefficient $\alpha \in \mathbb{R}$ that fits the data best, where we measure this fit by the norm of the residual, i.e. the squared difference between the approximation and the data. As a first step, we get $\rho_1 = \alpha_1 d_1$ consisting of a trial function $d_1 \in \mathcal{D}$ and a coefficient $\alpha_1 \in \mathbb{R}$ which are chosen such that the data misfit $\sum_{i=1}^{l}(y_i - \mathcal{F}^i(\alpha_1 d_1))^2$ is minimal. Then d_2 and α_2 are selected such that the residual is further minimized, i.e.

$$\begin{aligned} & \sum_{i=1}^{l}[(y_i - \mathcal{F}^i(\alpha_1 d_1)) - \mathcal{F}^i(\alpha_2 d_2)]^2 \\ = & \min_{\alpha\in\mathbb{R}, d\in\mathcal{D}} \sum_{i=1}^{l}[(y_i - \mathcal{F}^i(\alpha_1 d_1)) - \mathcal{F}^i(\alpha d)]^2. \end{aligned}$$

Generally, in every step the algorithm chooses d_n and α_n such that the norm of the residual

$$||R^n||^2_{\mathbb{R}^l} = ||y - \mathcal{F}\rho_n||^2_{\mathbb{R}^l} = \sum_{i=1}^{l}(y_i - \mathcal{F}^i\rho_n)^2$$

is minimized, where $\rho_n = \sum_{k=1}^{n} \alpha_k d_k$.
Since the inverse gravimetric problem is ill-posed, we need to use a regularization technique to get results that are stable with respect to noisy data. Here, we use a Tikhonov regularization, where the penalty term is concerned with the smoothness of the solution, i.e. we try to achieve a trade-off between fitting the data and reducing the $\mathrm{L}^2(\mathcal{B})$-norm of the solution. The regularization parameter λ correlates both terms. Thus, in step n we need to find the trial function d_{n+1} and the corresponding coefficient α_{n+1} such that they minimize

$$||R^n - \alpha_{n+1}\mathcal{F}d_{n+1}||^2_{\mathbb{R}^l} + \lambda||\rho_n + \alpha_{n+1}d_{n+1}||^2_{\mathrm{L}^2(\mathcal{B})},$$

where $\lambda > 0$ is the regularization parameter.
The Regularized Functional Matching Pursuit (RFMP) starts with $\rho_0 = 0$ (or some model), where the algorithm iteratively appends trial functions to the approximation of the unknown solution while trying to reduce the residual combined with some penalty term at each stage:

Algorithm 2.1 (RFMP)
Start with $\rho_0 := 0$ *(or some model) and* $R^0 = y$.
Given ρ_n.
Build $\rho_{n+1} := \rho_n + \alpha_{n+1} d_{n+1}$ *such that*

$$d_{n+1} \text{ maximizes } \left| \frac{\langle R^n, \mathcal{F}d \rangle_{\mathbb{R}^l} - \lambda \langle \rho_n, d \rangle_{\mathrm{L}^2(\mathcal{B})}}{\sqrt{||\mathcal{F}d||^2_{\mathbb{R}^l} + \lambda ||d||^2_{\mathrm{L}^2(\mathcal{B})}}} \right| \text{ and}$$

$$\alpha_{n+1} = \frac{\langle R^n, \mathcal{F}d_{n+1} \rangle_{\mathbb{R}^l} - \lambda \langle \rho_n, d_{n+1} \rangle_{\mathrm{L}^2(\mathcal{B})}}{||\mathcal{F}d_{n+1}||^2_{\mathbb{R}^l} + \lambda ||d_{n+1}||^2_{\mathrm{L}^2(\mathcal{B})}}.$$

Set $R^{n+1} = R^n - \alpha_{n+1} \mathcal{F} d_{n+1}$.

Code optimization and parallelization now allow a fast and competitive inversion of the data (see [13]). Note that the choice of the dictionary strongly affects the convergence rate of the method (see [12, 14] for further details). Thus, it is advantageous to choose a well-matched dictionary with respect to the structure of the solution. For our problem, we have some idea about the structure of the target function and impose this information on the choice of the dictionary.

2.4 The Dictionary

The algorithm chooses between four different types of trial functions: To reconstruct global trends it may use the polynomials $G^{\mathrm{I}}_{0,n,j}$. Note that there are two known systems of global orthonormal basis functions on $\mathcal{B}$, namely $G^{\mathrm{I}}_{m,n,j}$ and $G^{\mathrm{II}}_{m,n,j}$ (see, e.g., [23] and the references therein), where we decide to use the inner harmonics

$$G^{\mathrm{I}}_{0,n,j}(x) := \sqrt{\frac{2n+3}{a^3}} \left(\frac{|x|}{a} \right)^n Y_{n,j} \left(\frac{x}{|x|} \right), \quad x \in \mathcal{B},$$

where $n \in \mathbb{N}_0$ and $j = -n, \ldots, n$, since we only aim to recover the harmonic part of the density distribution.
The localized trial functions (wavelet-based scaling functions) $K^{\mathrm{I}}_h(\cdot, x)$ based on [1, 2, 3, 11, 23] for three different parameters h are, however, a very good choice to recover detail structures of the density distribution. Here, we use the parameter-dependent kernels

$$\tilde{K}^{\mathrm{I}}_h(y, x) := \sum_{n=0}^{E_n} \sum_{j=-n}^{n} h^n G^{\mathrm{I}}_{0,n,j}(x) G^{\mathrm{I}}_{0,n,j}(y), \quad x, y \in \mathcal{B},$$

where every fixed $h \in]0, 1[$ yields one particular kernel. The hat-width of such a kernel decreases for h getting closer to 1 (see figure 3). The peak of $y \mapsto \tilde{K}_h(y, x)$ is centred at x.

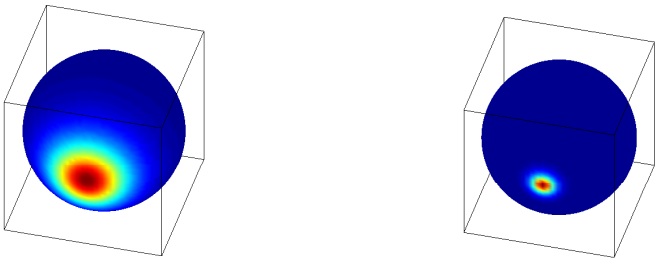

a) $h = 0.5$ b) $h = 0.8$

Figure 3: Kernel function $K_h^{\mathrm{I}}(\cdot, x)$ on the surface of the ball $\mathcal{B}$ with $h = 0.5$ and $h = 0.8$

In the following, we will always consider normalized kernel functions and denote them with $K_h^{\mathrm{I}}(\cdot, x)$, i.e.

$$K_h^{\mathrm{I}}(\cdot, x) := \frac{\tilde{K}_h^{\mathrm{I}}(\cdot, x)}{||\tilde{K}_h^{\mathrm{I}}(\cdot, x)||_{\mathrm{L}^2(\mathcal{B})}}.$$

Explicitly, the dictionary is now given as

$$\begin{aligned}\mathcal{D} := \quad & \left\{ K_h^{\mathrm{I}}(\cdot, x) \;\middle|\; h \in \{0.95, 0.96, 0.97\}, x \in \mathrm{grid}(\mathcal{B}) \right\} \\ & \cup \left\{ G_{0,n,j}^{\mathrm{I}} \;\middle|\; n = 3, \ldots, 11; j = -n, \ldots, n \right\},\end{aligned}$$

where $\mathrm{grid}(\mathcal{B})$ is a nearly quadratic grid, which is equiangular each in longitude and latitude. After the restriction to a spherical rectangle covering the Amazon area we are left with 39 800 grid points. Furthermore, we will stop the summation in the kernel functions after 100 summations, i.e. we set $E_n := 100$. This dictionary now contains approximately 120 000 elements of four different types.

3 Localizing extreme weather conditions in the Amazon area

We aim to invert the gravitational potential given by GRACE data for mass anomalies in the uppermost layer of the Earth. We may connect these mass redistributions with water mass transports close to the surface, i.e. with changes in the levels of ground, soil, or surface water, and snow packs. In this study, we observe the late sommer months of six consecutive years starting with 2005 in the Amazon area, where a large part is covered with rain forest. Thus, we do not convert the densities to, e.g., equivalent water heights.
To solve the inverse gravimetric problem with algorithm 2.1 (RFMP), we need

to apply the functionals $\mathcal{F}^k$ to the different types of trial functions:

$$\mathcal{F}^k G^{\mathrm{I}}_{m,n,j} = \delta_{m0}\ \tfrac{4\pi}{2n+1}\ \sqrt{\tfrac{a^3}{2n+3}}\ \left(\tfrac{a}{|x_k|}\right)^n\ \tfrac{1}{|x_k|}\ Y_{n,j}\left(\tfrac{x_k}{|x_k|}\right)$$

and

$$\begin{aligned}
\mathcal{F}^k K^{\mathrm{I}}_h(\cdot,x) &= \frac{1}{||\tilde{K}^{\mathrm{I}}_h(\cdot,x)||_{\mathrm{L}^2(\mathcal{B})}}\ \mathcal{F}^k \tilde{K}^{\mathrm{I}}_h(\cdot,x) \\
\mathcal{F}^k \tilde{K}^{\mathrm{I}}_h(\cdot,x) &= \sum_{n=0}^{E_n} h^n\ \left(\frac{|x|}{|x_k|}\right)^n\ \frac{1}{|x_k|}\ P_n\left(\frac{x}{|x|}\cdot\frac{x_k}{|x_k|}\right)
\end{aligned}$$

$$||\tilde{K}^{\mathrm{I}}_h(\cdot,x)||_{\mathrm{L}^2(\mathcal{B})} = \sum_{n=0}^{E_n} h^{2n}\ \frac{2n+3}{a^3}\ \frac{2n+1}{4\pi}\ \left(\frac{|x|}{a}\right)^{2n}.$$

We use the dictionary $\mathcal{D}$, where the series in the kernel functions is terminated at degree 100. Moreover, we stop algorithm 2.1 (RFMP) after 20 000 iterations. We invert the potential values $y_i = V_a(x_i) - V_{\mathrm{mean}}(x_i)$ at 23 350 data points x_i, where V_a is the mean potential of the summer months (July to October) for each of the years $a = 2005, \ldots, 2010$ denoised with a cubic polynomial (cp) filter ψ_J, where J is chosen as suggested in section 2.2, and V_{mean} is the mean value of all these V_a. The data grid is similarly structured like grid($\mathcal{B}$) but is located 7 km above the Earth's surface. Numerical tests suggested $\lambda = 10$ to be a good regularization parameter, that allows for a smooth reconstruction of the signal without a too large attenuation. We use the same regularization parameter for all months to keep comparability. Note that we resolve the solution on a grid of approximately 0.15 degrees latitude times 0.2 degrees longitude, which is a very high resolution. Furthermore, we solve for the density in g/cm^3, since GRACE data is of limited value in the Amazon area when forming quantitative estimates (e.g. in mm).

In figure 4, we display the resulting density deviations for summer 2005 to summer 2010. The colour blue denotes that the humidity is higher than in the mean, i.e. the surface and ground water levels are higher than in the mean, while red denotes that the humidity is lower than in the mean. We clearly observe the extreme weather events of these six years in our results, i.e. the droughts in 2005 and 2010 and the remainders of the flood in spring 2009. Furthermore, we can locate these events much more accurately than before (confer sections 4 and 5). The main signal in 2005 is located on a stream bifurcation, where the Negro river meets the main stream. In 2010 the main signal is located exactly on the Xingu river and the main stream. In 2009, we clearly see the remainders of the flood in spring in the area of the main stream of the Amazon. Moreover, we already see the beginnings of the drought in Venezuela, especially in the area of the Orinoco river in the north of South America, which lead to major energy problems in the following winter. Such a level of resolution for extreme weather conditions in the case of inverted satellite data alone is a direct consequence

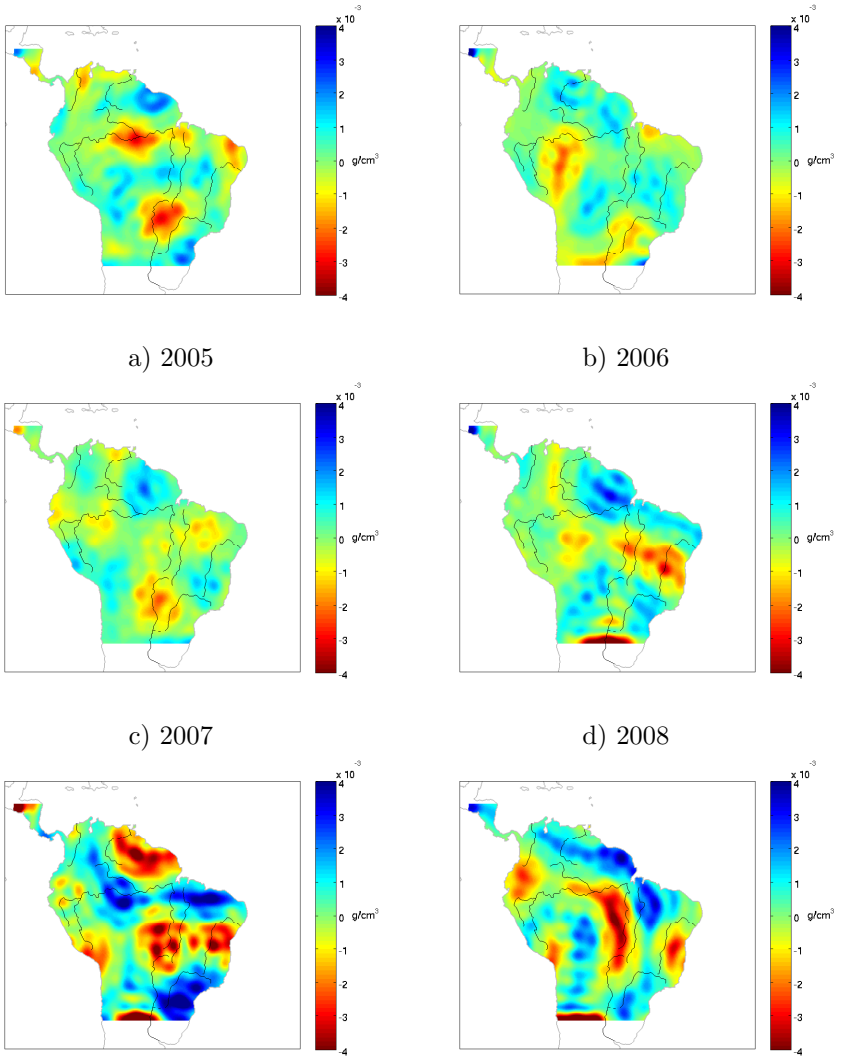

a) 2005 b) 2006

c) 2007 d) 2008

e) 2009 f) 2010

Figure 4: Density deviations for late summer of the years 2005 to 2010 computed with the RFMP out of 25 440 data points for the filtered GRACE gravity potential (as discussed in section 2.2) and a regularization parameter $\lambda = 10$. For each of the six computations, the RFMP was stopped after 20 000 iterations. The resolution is 0.15 degrees latitude times 0.2 degrees longitude. The consequences of the droughts in 2005 and 2010 and the flood in 2009 are clearly visible and localized.

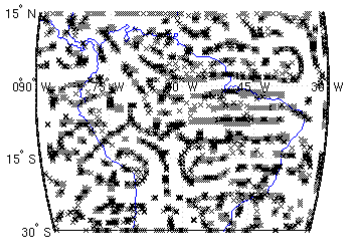

Figure 5: Centre points x of the chosen localized trial functions $K_h^{\mathrm{I}}(\cdot, x)$ computed with the RFMP out of 25 440 data points for late summer 2010 in the case of the inversion of the filtered GRACE gravity potential and a regularization parameter $\lambda = 10$. The RFMP was stopped after 20 000 iterations. The choice of the centres is automatically correlated with the main structures in the solution.

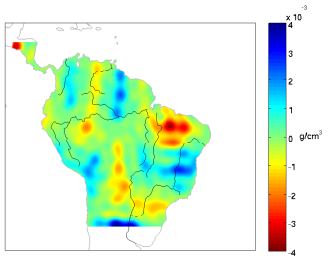

Figure 6: Density deviation for late summer of the years 2007 computed with the RFMP out of 25 440 data points for the filtered GRACE gravity potential and a regularization parameter $\lambda = 10$. The data is filtered with a too large parameter $J = \frac{\ln 25}{\ln 2}$. The RFMP was stopped after 20 000 iterations.

of using the novel method introduced in this work and involving localized trial functions. As an example, we display the centres x of the chosen localized kernel functions $K_h(\cdot, x)$ for summer 2009 in figure 5. Clearly, the expansion functions are primarily chosen where the detail density of the solution is highest (confer figure 4 f)). For more information about the theoretical properties of algorithm 2.1 (RFMP) and further numerical case studies on the mass transports in the Amazon area derived from GRACE data as well as the density distribution in the area of South America or the Himalayas out of the EGM2008, we refer to [12, 13, 14].

As discussed in section 2.2, we filter the input with respect to the signal to noise ratio of the data. Let us, as an example, display the consequences of this decision on the solution of the year 2007. Note that we already discussed the input of this particular year (see figure 2). In figure 6, we display the solution

of the inversion of an input filtered with the too large parameter $J = \frac{\ln 25}{\ln 2}$. Clearly, we recover mostly stripes that are noise in form of the satellite tracks of the GRACE satellites. In comparison, the solution corresponding to an input filtered with $J = \frac{\ln 23}{\ln 2}$ (see figure 4 c)) gives a result that is not disturbed by this kind of noise.

4 Comparison to Traditional Filtering of GRACE Data

Let us compare our results to results gained with other methods. In [7], the drought of 2005 was observed in a series of six consecutive years starting with 2002 out of the same data that we use here for the months August and September of each of these years. After two steps of filtering (removing correlated noise and smoothing with a 500-km Gaussian filter, see [6] as well) and removing the mean of these months, one gets the variations of the gravity field, expressed in equivalent water heights in cm on a grid of 1×1 degrees. In figure 1 in [7] mass changes are displayed over South America for August/September of the years 2002 to 2007. Thus, we may compare the results of the years 2005 to 2007 qualitatively to our results. Note that in [7] the colour bar is inverted, i.e. blue denotes that the humidity is lower than in the mean while red denotes that the humidity is higher than in the mean. Although in both time series the drought of 2005 can be identified, it is much more localized when using the RFMP.

5 Comparison to Other Data

First, we want to compare our results to the NOAA-CIRES Twentieth Century Global Reanalysis Version II data provided by the NOAA/OAR/ESRL PSD, Boulder, Colorado, USA, on their Web site at http://www. esrl.noaa.gov/psd. The data is given from the year 1948 until present and assimilates only surface observations of synoptic pressure, monthly sea surface temperature, and sea ice distribution. The volumetric soil moisture content in the first 100 cm is given on a grid of approximately 2 degrees latitude times 2 degrees longitude.
Secondly, we compare our results to the average layer 1 soil moisture given by the monthly gridded GLDAS Noah Land Surface Model L4 Monthly 0.25 x 0.25 degree which contains a series of land surface parameters simulated from the Noah 2.7.1 model in the Global Land Data Assimilation System (GLDAS) in 0.25 degree resolution ranging from 2000 to the present (confer [25]). The data consists of monthly averaged densities in kg/m^2 of the top 100 cm. Note that the data is based on a model.

In figures 7 (volumetric soil moisture content) and 8 (average layer 1 soil moisture for the top 100 cm), we display the results of both for the late summer months (July to October) of the years 2005 to 2010 as a difference to the respective mean of all these months (as was done for the GRACE data before). Note that the resolution of the volumetric soil moisture content is relatively low

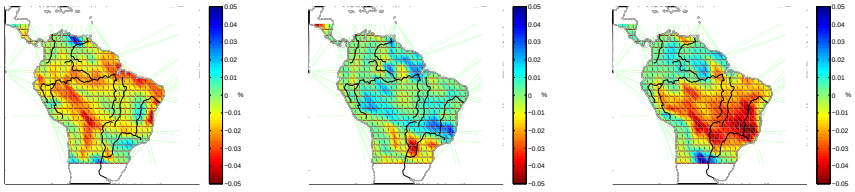

a) 2005 b) 2006 c) 2007

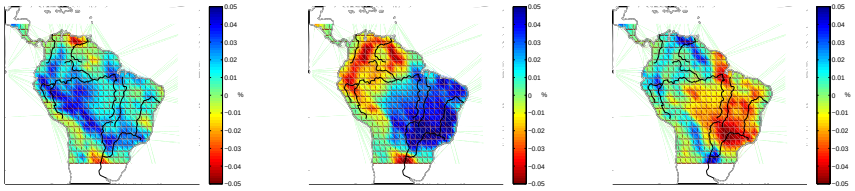

d) 2008 e) 2009 f) 2010

Figure 7: The volumetric soil moisture content in the first 100 cm for late summer of the years 2005 to 2010 as given by the 20th Century Reanalysis V2 data. The resolution is 2 degrees latitude times 2 degrees longitude.

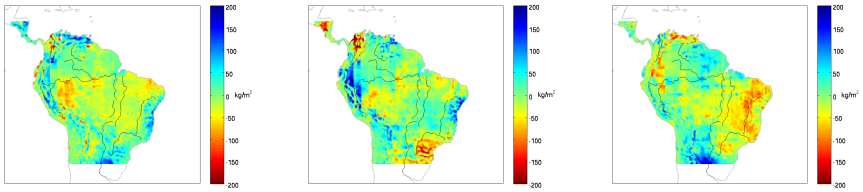

a) 2005 b) 2006 c) 2007

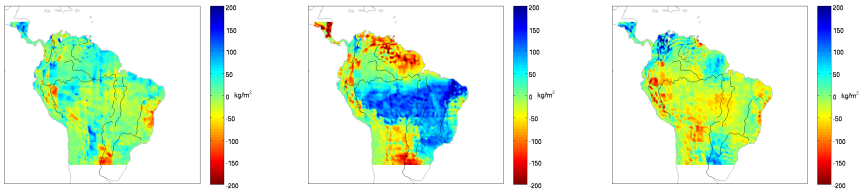

d) 2008 e) 2009 f) 2010

Figure 8: The average layer soil moisture for the top 100 cm for late summer of the years 2005 to 2010 as given by the GLDAS/NOAH data. The resolution is 0.25 degrees latitude times 0.25 degrees longitude.

(2×2 degrees both in latitude and longitude) while the average layer 1 soil moisture is given on a grid of 0.25 degrees latitude times 0.25 degrees longitude. However, the second one is a model and not given by measured data.
Nonetheless, we detect the same climate phenomena as in the results from the inversion of GRACE data. In 2005 and 2010, we can observe a drought while we see in 2009 the remainders of a flood in spring 2009 and the beginnings of the drought in winter 2009 in the Orinoco basin. Both data sets do not show any large signals in 2006. However, the volumetric soil moisture content appears to overestimate the climate situations in 2007 (there seems to be a drought) and 2008 (there seems to be a flood) both. Neither the results from inverted GRACE data nor the average layer 1 soil moisture (or any other media) report such events.
The average layer 1 soil moisture appears to illustrate the weather situation in the Amazon area in late summer more accurately and with a better resolution than the volumetric soil moisture content given by measured data. However, although the inverted GRACE data as well as the soil moisture model show the same events very clearly, the mass anomalies inverted from GRACE data show a much better resolution and seem to locate the events far better (see the main signal of the drought in 2005 located on a stream bifurcation or the beginnings of the 2009 drought in the Orinoco area).
Note that a comparison of GRACE data and hydrological data in [6] also discovered the poor quality of the hydrological data with respect to extreme weather events. However, there are still no means to directly validate the GRACE data.

6 Conclusions and Outlook

We presented a novel method called the RFMP to locate climate effects like droughts or floods in inverted satellite data. This method allows the inversion of noisy data with a very good spatial resolution by mixing different types of trial functions, e.g., functions with a global character as well as localized functions. Furthermore, in [12, 13, 14] it was shown that the method is well-matched to invert heterogeneous data as well as large data sets.
Here we presented a study of the extreme weather conditions in the late summer months in the Amazon area in recent years. The RFMP clearly reconstructs the droughts 2005 and 2010 as well as the remainders of a flood in spring 2009. Furthermore, we can, for example, locate the origin of a dry spot close to a stream bifurcation, which is very plausible. Thus, in comparison to other methods and data, we reach a new level of resolution of these effects.
Moreover, the method showed great potential in analyzing ecologically relevant problems. We expect it to be applicable to the analysis of similar mass transports such as the deglaciation as well. Furthermore, the characteristics of the RFMP promise a great potential in the combination of satellite data and Earth-bound data to get an approximation with even higher accuracy and resolution.

Acknowledgement 6.1 *We gratefully acknowledge the support by the German Research Foundation (DFG), projects MI 655/2-2 and MI 655/7-1. Furthermore, we are grateful that Abel Amirbekyan (Fraunhofer ITWM Kaiserslautern) helped us to optimize and parallelize our code.*
GRACE land data were processed by Sean Swenson, supported by the NASA MEaSUREs Program, and are available at http://grace.jpl.nasa.gov.
The NOAA-CIRES Twentieth Century Global Reanalysis Version II data for this study are from the Research Data Archive (RDA) which is maintained by the Computational and Information Systems Laboratory (CISL) at the National Center for Atmospheric Research (NCAR). NCAR is sponsored by the National Science Foundation (NSF). The original data are available from the RDA (http://dss.ucar.edu) in dataset number ds131.1.
The GLDAS/NOAH data used in this study were acquired as part of the mission of NASA's Earth Science Division and archived and distributed by the Goddard Earth Sciences (GES) Data and Information Services Center (DISC).

References

[1] Amirbekyan A, Michel V (2008) Splines on the three-dimensional ball and their application to seismic body wave tomography. Inverse Problems 24:1–25

[2] Berkel P (2009) Multiscale methods for the combined inversion of normal mode and gravity variations. Dissertation, Geomathematics Group University of Kaiserslautern (Aachen: Shaker Verlag)

[3] Berkel P, Michel V (2010) On mathematical aspects of a combined inversion of gravity and normal mode variations by a spline method. Math Geosci 42:795–816

[4] Chen J L, Wilson C R, Tapley B D (2006) Satellite gravity measurements confirm accelerated melting of Greenland ice sheet. Science 313:1958–60

[5] Chen J L, Wilson C R, Tapley B D, Blankenship D D, Young D (2008) Antarctic regional ice loss rates from GRACE. Earth Planet Sci Lett 266:140–8

[6] Chen J L, Wilson C R, Tapley B D, Grand S (2007) GRACE detects coseismic and postseismic deformation from the Sumatra-Andaman earthquake. Geophys Res Lett 34:L13302

[7] Chen J L, Wilson C R, Tapley B D, Yang Z L, Niu G Y (2009) 2005 drought event in the Amazon river basin as measured by GRACE and estimated by climate models. J Geophys Res 114:B05404

[8] Chen J L, Wilson C R, Tapley B D (2010) The 2009 exceptional Amazon flood and interannual terrestrial water storage change observed by GRACE. Water Resour Res 46:W12526

[9] Crowley J W, Mitrovica J X, Bailey R C, Tamisiea M E, Davis J L (2006) Land water storage within the Congo Basin inferred from GRACE satellite gravity data. Geophys Res Lett 33:L19402

[10] Fengler M J, Freeden W, Kohlhaas A, Michel V, Peters T (2007) Wavelet modeling of regional and temporal variations of the Earth's gravitational potential observed by GRACE. J Geodesy 81:5–15

[11] Fengler M J, Michel D, Michel V (2006) Harmonic spline-wavelets on the 3-dimensional ball and their application to the reconstruction of the Earth's density distribution from gravitational data at arbitrarily shaped satellite orbits. ZAMM 86:856–73

[12] Fischer D (2011) Sparse regularization of a joint inversion of gravitational data and normal mode anomalies. Dissertation, Geomathematics Group University of Siegen (München: Verlag Dr. Hut)

[13] Fischer D, Michel V (2012) How to combine spherical harmonics and localized bases for regional gravity modelling and inversion. http://www.uni-siegen.de/fb6/geomathe/preprints/spg_8.pdf. Accessed 11 June 2012

[14] Fischer D, Michel V (2012) Sparse regularization of inverse gravimetry – case study: spatial and temporal mass variations in South America. Inverse Problems 28:065012

[15] Freeden W, Gervens T, Schreiner M (1998) Constructive approximation on the sphere (with applications to geomathematics). Oxford University Press, Oxford

[16] Freeden W, Windheuser U (1996) Spherical wavelet transform and its discretization. Adv Comput Math 5:51–94

[17] GRACE overview: Center for Space Research, University of Texas (Austin). www.csr.utexas.edu/grace/overview.html. Accessed 11 June 2012

[18] Hu X G, Chen J L, Zhou Y H, Huang C, Liao X H (2006) Seasonal water storage change of the Yangtze River basin detected by GRACE. Sci China Ser D Earth Sci 49:483–91

[19] JPL: Jet Propulsion Laboratory, California Institute of Technology (Pasadena). http://podaac.jpl.nasa.gov/grace/index.html. Accessed 11 June 2012

[20] Kusche J (2007) Approximate decorrelation and non-isotropic smoothing of time-variable GRACE-type gravity field models. J Geodesy 81:733–49

[21] Kusche J, Schmidt R, Petrovic S, Rietbroek R (2009) Decorrelated GRACE time-variable gravity solutions by GFZ, and their validation using a hydrological model. J Geodesy 83:903–13

[22] Michel V (2002) A multiscale approximation for operator equations in separable Hilbert spaces – case study: reconstruction and description of the Earth's interior. Habilitation, Geomathematics Group University of Kaiserslautern (Aachen: Shaker Verlag)

[23] Michel V (2010) Tomography: problems and multiscale solutions. In: Freeden W et al (ed) Handbook of Geomathematics. Heidelberg, Springer, pp 949–72

[24] Michel V, Fokas A S (2008) A unified approach to various techniques for the non-uniqueness of the inverse gravimetric problem and wavelet-based methods. Inverse Problems 24:045091

[25] Rodell M et al (2004) The global land data assimilation system. Bull Am Meteorol Soc 85:381–94

[26] Rodell M, Familiglietti J S, Chen J, Seneviratne S I, Viterbo P, Holl S, Wilson C R (2004) Basin scale estimates of evaporation using GRACE and other observations. Geophys Res Lett 31:L20504

[27] Syed T H, Famiglietti J S, Chen J, Rodell M, Seneviratne S I, Viterbo P, Wilson C R (2005) Total basin discharge for the Amazon and Mississippi River basins from GRACE and a land-atmosphere water balance. Geophys Res Lett 32:L24404

[28] Tapley B D, Bettadpur S, Ries J C, Thopson P F, Watkins M M (2004) GRACE measurements of mass variability in the Earth system. Science 305:503–5

[29] Wahr J, Swenson S, Velicogna I (2006) The accuracy of GRACE mass estimates. Geophys Res Lett 33:L06401

[30] Winsemius H C, Savenije H H G, van de Giesen N C, van den Hurk B J J M, Zapreeva E A, Klees R (2006) Assessment of gravity recovery and climate experiment (GRACE) temporal signature over the upper Zambezi. Water Resour Res 42:W12201

Siegen Preprints on Geomathematics

The preprint series “Siegen Preprints on Geomathematics” was established in 2010. See www.geomathematics-siegen.de for details and a contact address. At present, the following preprints are available:

1. P. Berkel, D. Fischer, V. Michel: *Spline multiresolution and numerical results for joint gravitation and normal mode inversion with an outlook on sparse regularisation*, 2010.
2. M. Akram, V. Michel: *Regularisation of the Helmholtz decomposition and its application to geomagnetic field modelling*, 2010.
3. V. Michel: *Optimally Localized Approximate Identities on the 2-Sphere*, 2010.
4. N. Akhtar, V. Michel: *Reproducing Kernel Based Splines for the Regularization of the Inverse Spheroidal Gravimetric Problem*, 2011.
5. D. Fischer, V. Michel: *Sparse Regularization of Inverse Gravimetry - Case Study: Spatial and Temporal Mass Variations in South America*, 2011.
6. A.S. Fokas, O. Hauk, V. Michel: *Electro-Magneto-Encephalography for the three-Shell Model: Numerical Implementation for Distributed Current in Spherical Geometry,* 2011.
7. M. Akram, I. Amina, V. Michel: *A Study of Differential Operators for Complete Orthonormal Systems on a 3D Ball*, 2011.
8. D. Fischer, V. Michel: *How to combine spherical harmonics and localized bases for regional gravity modelling and inversion*, 2012.
9. D. Fischer, V. Michel: *Inverting GRACE gravity data for local climate effects,* 2012.

Geomathematics Group Siegen
Prof. Dr. Volker Michel

Contact at:
Geomathematics Group
Department of Mathematics
University of Siegen
Walter-Flex-Str. 3
57068 Siegen
www.geomathematics-siegen.de

UNIVERSITÄT SIEGEN